Energy spectra of tailored particle beams from trapped single-component plasmas[a)]

T. R. Weber, J. R. Danielson,[b)] and C. M. Surko
Department of Physics, University of California San Diego, La Jolla, California 92093-0319, USA

(Received 5 December 2008; accepted 9 March 2009; published online 11 May 2009)

A nondestructive technique was developed recently to create beams of electrons (or positrons) with small transverse spatial extent and high brightness from single-component plasmas confined in a Penning–Malmberg trap [T. R. Weber *et al.*, Phys. Plasmas **90**, 123502 (2008)]. A model for beam extraction was developed that successfully predicts the resulting beam profiles. This model is used here to predict the beam amplitudes and the energy distribution of the beams as a function of the exit-gate voltage. The resulting expressions, suitably scaled by the plasma parameters, depend only on the exit-gate voltage and the electrode radius. Predictions of the theory are confirmed using electron plasmas. This technique permits the formation of beams with both small transverse spatial extent and small energy spread. Applications involving antimatter beams (e.g., positrons) are discussed, including bright beams for improved spatial resolution, short pulses for time-resolved studies, and cold beams for improved energy resolution. © *2009 American Institute of Physics*. [DOI: 10.1063/1.3110109]

I. INTRODUCTION

Charged particle beams are useful in a wide range of applications in science and technology.[1–5] In the case of common particles such as electrons, beams generated by a simple heated cathode are adequate for many applications. However, when the particles are more difficult to obtain, as is the case with positrons and antiprotons, more refined techniques are required. In this case, it has proven convenient to use trap-based beams, where the particles are first accumulated efficiently and cooled in an electromagnetic trap, then a beam or pulse of particles is extracted.[5–9] In recent work, which provides the starting point for this paper, a Penning–Malmberg trap was used to create high-quality, trap-based beams.[10,11] The technique is illustrated in Fig. 1. Rotating electric fields are used to compress plasmas radially, and then the confining, end-gate potential is lowered carefully to extract a beam from the center of the trapped plasma (i.e., where the space charge potential is largest). The processes of plasma cooling, radial plasma compression, and beam extraction can all be accomplished nondestructively with nearly 100% efficiency making this method particularly useful for the formation of tailored beams of antimatter.

The work presented here focuses on the further development of this technique to create tailored, high-quality beams by extraction from plasmas in a Penning–Malmberg trap. It is shown that this method of the formation of beams with small transverse spatial extent is a true brightness enhancing process. Specifically, it preserves the narrow energy spread of the beam, which, in turn, is set by the plasma temperature. Such beams are expected to be useful in many applications. For example, the creation of beams with small transverse energy spread and small transverse spatial extent is critical in the development of positron microscopic techniques to study materials.[2,12] In another application, beams with small total energy spread will enable new kinds of spectroscopic studies of positron interactions with matter such as higher resolution studies of the positron-impact excitation of vibrational and rotational transitions in molecules.[13–15] Similarly, beams with narrow parallel energy spread will facilitate pulse compression in the time domain. This, in turn, could enable the development of new techniques for positron annihilation lifetime spectroscopic (PALS) studies of materials.[16–23] Another important application of tailored positron sources is the creation of cold antihydrogen atoms,[24,25] one goal of which is to test fundamental theories of nature (e.g., the CPT theorem which requires the invariance of field theories under charge conjugation, parity inversion and time reversal). As discussed at the end of this paper, beams with small transverse spatial extent and small total energy spread could potentially enable new scenarios to create these cold antiatoms.

As we discuss below, a key parameter determining the beam properties in the regime studied here is the scaled beam-pulse amplitude

$$\xi = \frac{e^2 N_b}{T L_p}, \tag{1}$$

where N_b is the number of beam particles extracted and L_p is the plasma length.[11] Physically, ξ is the change in the plasma potential across the beam due to the extracted beam particles, scaled to plasma temperature T. A central result of Refs. 10 and 11 is that, for small beams (i.e., small number of beam particles, $\xi \ll 1$), the radial beam profile is Gaussian with a minimum full width to $1/e$ of $4\lambda_D$, where λ_D is the Debye length.[11] Experimentally, we find that as ξ increases, the beam width also increases. As discussed below, this is due to the fact that the exiting particles flatten the potential profile near the plasma center.

[a)]Paper TI1 5, Bull. Am. Phys. Soc. **53**, 239 (2008).
[b)]Invited speaker.

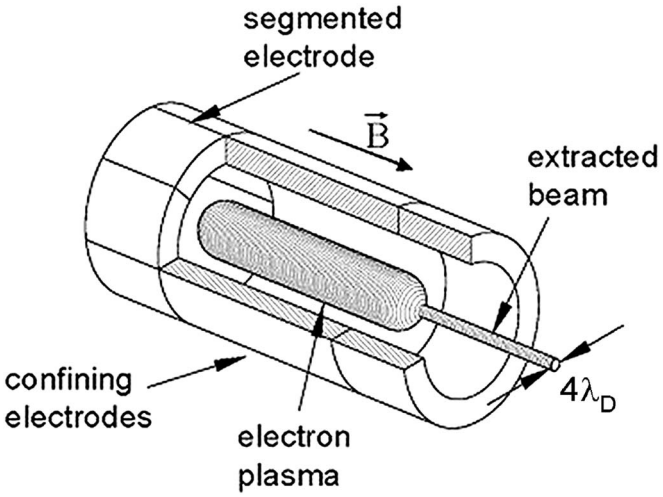

FIG. 1. Simplified schematic diagram of the technique used to extract beams with small transverse spatial extent from single-component plasmas in a Penning–Malmberg trap.

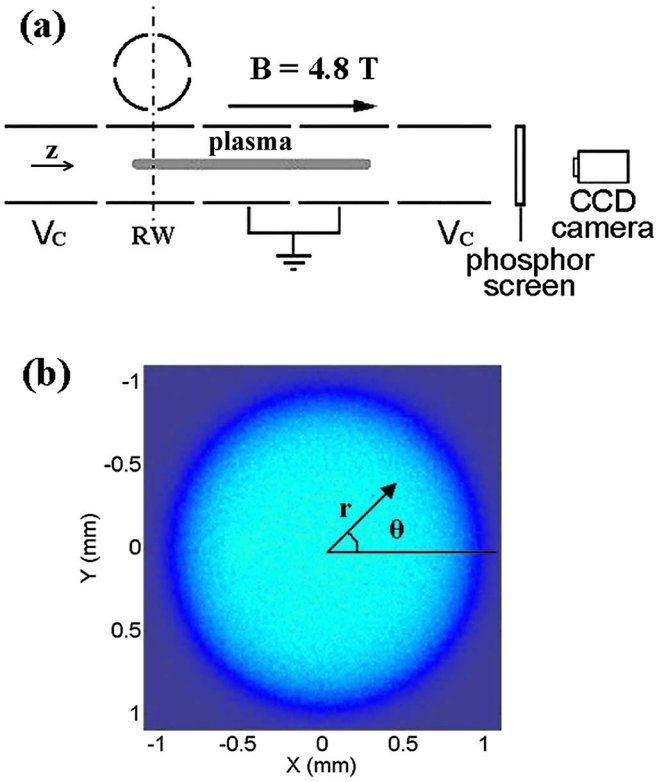

FIG. 2. (Color online) (a) Schematic diagram of the experimental arrangement and (b) a CCD image of the areal plasma density $\sigma_z(r,\theta)$ for an equilibrium flat-top plasma.

This paper focuses on the energy distributions of the particles extracted using this technique. Although the beam energy distribution is simply the energy distribution of the plasma particles that can escape, it contains a dependence on the changing plasma potential $\phi(r)$. Because of this, it has a nontrivial dependence on ξ (or equivalently N_b). A simple model for beam extraction is used to derive an expression that accurately predicts ξ for a given plasma and end-gate extraction voltage V_E. Using this expression, the beam energy distribution $f(E_\parallel)$ as a function of $E_\parallel$, the kinetic energy of the beam particles in motion parallel to the magnetic field, is derived for given values of ξ (which is set by V_E). Other parameters of interest including the root-mean-square (rms) spread (i.e., the dispersion) in the total energy of the beam ΔE and changes in the shape of the distribution function as a function of ξ are also discussed.

II. PENNING–MALMBERG TRAP FOR BEAM FORMATION

Plasma particles are accumulated and stored in a Penning–Malmberg trap, shown schematically in Fig. 2(a).[11] It consists of a set of cylindrical electrodes of inner radius $R_W=1.27$ cm in a uniform magnetic field of strength $B=4.8$ T. The particles are confined radially by the magnetic field and axially by voltages V_C, applied to electrodes at each end. The resulting plasma is in thermal equilibrium at temperature T. The plasma is a uniform density rigid rotor rotating at an $E\times B$ frequency, $f_E=cn_0e/B$, where n_0 is the equilibrium plasma density. The plasma parameters are z-independent, thus making r and θ the coordinates of interest.

The principal diagnostic used here is a digital camera and a phosphor screen, located outside of the trap, to image the two-dimensional (i.e., areal) plasma density distribution. By quickly reducing V_C on one end of the plasma to zero, the plasma particles stream out of the trap along the magnetic field. They are then accelerated to energies of 5 keV and then impinge on a phosphor screen. The resulting fluorescent light is imaged to obtain the z-integrated areal plasma density profile $\sigma_z(r,\theta)$. A typical image is shown in Fig. 2(b). The plasma density n is then given by $n(r,\theta)=\sigma_z(r,\theta)/L_p$, where L_p is the plasma length. The magnetic field decreases adiabatically from the end of the trap to the phosphor screen, causing the beam to increase by a factor of 5 when it is imaged. However, all measurements in this work refer to the beam while it is still in the trap.

To extract a beam from a trapped plasma, V_C at one end of the plasma is lowered to a value V_E for about 15 μs. This process is illustrated schematically in Fig. 3(a) where the potential at $r=0$ is shown during an extraction. The extraction time is chosen to be sufficiently long so that particles with sufficient energy have ample time to escape, but short enough so that the effects of collisions, instabilities, and radial transport are negligible. Because the plasma potential is highest at the (radial) plasma center, the beam emanates from this region. This is then used to create beams with spatial extents much smaller than those of the original plasma. Shown in Fig. 4 are examples of radial profiles of extracted beams for two values of ξ. Figure 3(b) shows images of a plasma before and after a beam is extracted. Notice the small hole at the center, illustrating the location of the particles that exited the trap. This hole moves to the plasma edge and disappears in a time=500 μs which, in turn, may permit pulsed-beam extraction at kilohertz rates.

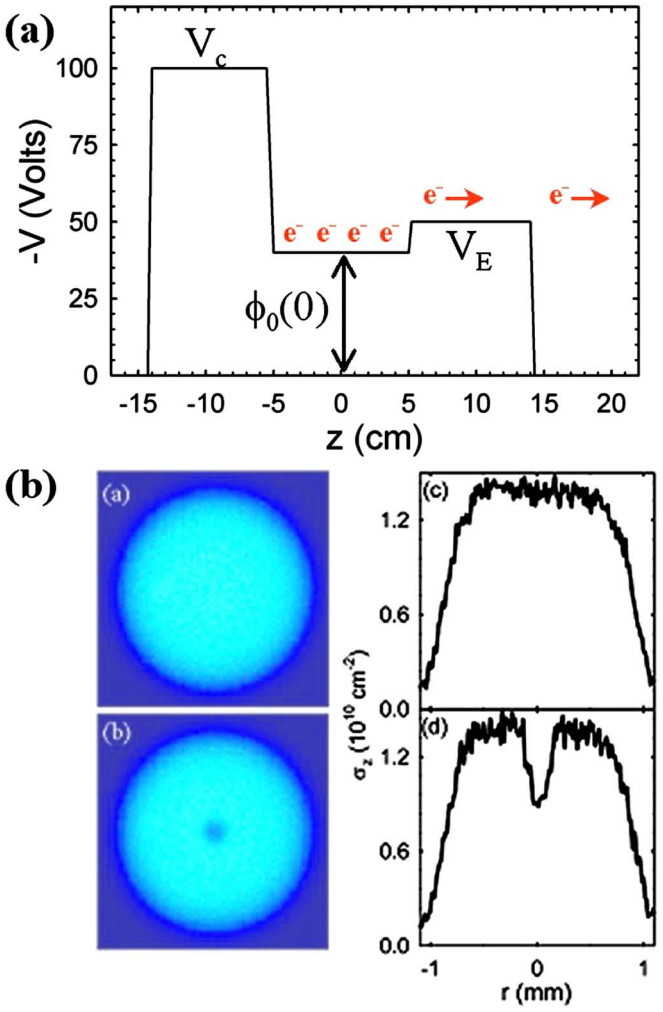

FIG. 3. (Color online) (a) Schematic diagram of the beam extraction process and (b) camera images of the areal plasma density $\sigma_z(r,\theta)$ for a flat-top plasma before beam extraction (above) and 10 μs after beam extraction (below); also shown are the radially corresponding averaged slice distributions $\sigma_z(r)$.

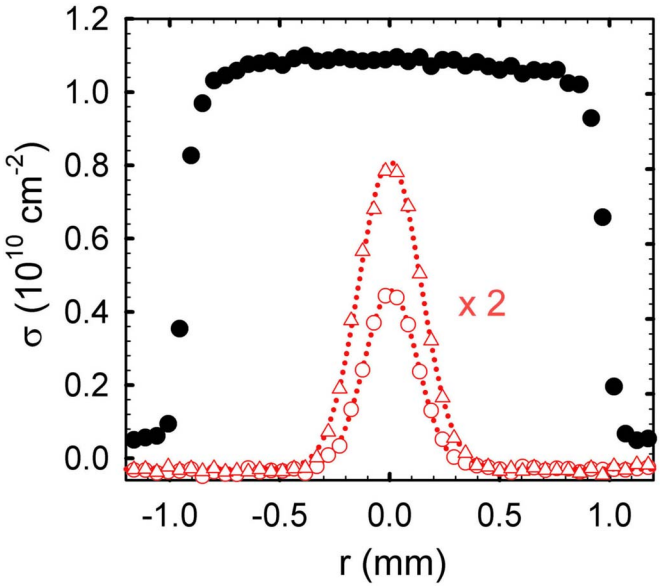

FIG. 4. (Color online) Shown are the areal radial distribution functions $\sigma_b(r)$ for electron beams with amplitudes $\xi \approx 0.02$ and 0.5 plotted with open circles and triangles, respectively. A Gaussian fit $(\cdots)$ to the beam distributions indicates half widths to $1/e$ of $\rho_b \approx 2.2\lambda_D$ and $2.6\lambda_D$, respectively. The z-integrated areal density distribution $\sigma_z(r)$ of the initial plasma (solid circles) is also shown.

III. THEORETICAL CONSIDERATIONS

In this section, an expression is developed for the energy distribution of the beam particles as a function of ξ which, in an experiment, is set by V_E. As mentioned above, it is assumed that the exit gate is lowered for a time Δt, which is sufficiently long so that all particles with enough energy to escape do so. It is also assumed that at a given radius, particles escape in the order of $E_\parallel$ such that the particles with largest $E_\parallel$ escape first and those with smallest $E_\parallel$ escape last. While not strictly valid, this assumption makes the calculations below tractable and is qualitatively correct in that the particles with large $E_\parallel$ traverse the plasma length faster than particles with small $E_\parallel$, and thus they are likely to escape first. The finite slewing time of the exit-gate electrode also favors this order.

When the end-gate potential is lowered to V_E and the particles begin to escape, the potential near the center of the plasma changes in such a way as to inhibit further particles from leaving. We denote $\phi_0(r)$ and $n_0(r)$ as the equilibrium plasma potential and density, and $\Delta\phi(r)$ and $\Delta n(r)$ as the change in the plasma potential and density from equilibrium due to the extracted beam particles. After extraction, the new density and space-charge potential profiles are $n(r)=n_0(r)-\Delta n(r)$ and $\phi(r)=\phi_0(r)-\Delta\phi(r)$, respectively. A similar theoretical description has been used previously to evaluate the effect of space charge on measurement of the plasma temperature.[26–28] In contrast, as stated above, this paper evaluates explicitly the effect of the space charge on the energy distribution of the escaping particles.

The condition that a particle escapes is $E_\parallel > -eV_E$, where $E_\parallel$ is the kinetic energy outside of the trap of a beam particle in the motion parallel to the magnetic field and V_E is the extraction voltage referenced to ground potential outside the trap (i.e., 0 V). When an electron escapes from the plasma to a region of zero potential, it does so along a magnetic field line at a constant radius. The energy $E_\parallel$ is a sum of the kinetic and potential energy of the particle in the plasma before it escaped. With this in mind, the single particle distribution function for a "flat-top" plasma in thermal equilibrium is approximately

$$f_P(E_\parallel, E_\perp, r, \theta, z) \approx \frac{n_0(r)}{\sqrt{\pi}T^{3/2}} \frac{\exp\left(-\dfrac{E_\perp + E_\parallel + e\phi(r)}{T}\right)}{\sqrt{E_\parallel + e\phi(r)}}, \qquad (2)$$

where the uniform $E \times B$ rotation has been neglected, an assumption valid when the thermal velocity is much greater then the rotation velocity at the edge of the beam. For small beams $(\rho_b = 2\lambda_D)$, the condition for this assumption can be written as $w_p^2/w_c^2 \ll 1$ and is satisfied for all plasmas far from the Brillouin limit. For the plasmas in this work, $w_p^2/w_c^2 \ll 1 \times 10^{-5}$.

Here, $E_\perp$ is the kinetic energy of a beam particle in the motion perpendicular to the magnetic field, which is assumed to remain constant during the beam extraction process. In the plasma, the kinetic energy of a particle in the motion parallel to the magnetic field is $E_\parallel + e\phi_0(r)$. When a beam is extracted from the plasma to a region of zero potential, the energy distribution of the beam is given by Eq. (2) integrated over r, θ, and z with the additional constraint that $E_\parallel > -eV_E$. However, the dependence of $\Delta\phi(r)$ on the number of escaping particles makes the calculation of this integral nontrivial. For sufficiently small beams, $\Delta\phi(r)$ can be neglected so that $\phi(r) \approx \phi_0(r)$ and is independent of ξ. The potential $\phi_0(r)$ can be calculated analytically and is quadratic in r (i.e., inside the constant-density plasma).[11] Integration over the spatial variables is then tractable. This and integration over $E_\perp$ yield for parallel-energy distribution

$$f(E_\parallel) = \frac{L_p}{e^2}\mathrm{erfc}\left[\frac{E_\parallel + e\phi_0(0)}{T}\right], \tag{3}$$

where erfc is the complementary error function for values of $E_\parallel > V_E$; $f(E_\parallel)=0$ for $E_\parallel < V_E$. It is related to the full energy distribution (i.e., including $E_\perp$) by $f(E_\parallel, E_\perp) = f(E_\parallel)e^{-E_\perp/T}/T$.

When $[E_\parallel + e\phi_0(r)]/T \geq 2$, Eq. (3) can be approximated by

$$f(E_\parallel) \approx \frac{L_p\sqrt{T}}{e^2\sqrt{\pi}}\frac{\exp(-[E_\parallel + e\phi_0(0)]/T)}{\sqrt{E_\parallel + e\phi_0(0)}}. \tag{4}$$

This is the approximate energy distribution for small beams (i.e., when $\xi \ll 1$). Equation (4) is just the tail of a Maxwellian energy distribution starting at energy of $-e\phi_0(0)$.

For larger beam amplitudes, $\Delta\phi(r)$ cannot be neglected. In previous work[11] it was shown that for $\xi < 1$, radial beam profiles extracted in this way are Gaussian distributions with widths given by

$$\rho_b = 2\lambda_D(1+\xi)^{1/2}. \tag{5}$$

The change in potential in the plasma $\Delta\phi(r)$ can be calculated analytically for a Gaussian beam

$$\Delta\phi(r) = \frac{T\xi}{e}\left[2\ln\frac{r}{R_W} + \Gamma\left(0, \frac{r^2}{\rho_b^2}\right) - \Gamma\left(0, \frac{R_W^2}{\rho_b^2}\right)\right]$$
$$\approx \Delta\phi(0) + \xi\frac{T}{e}\frac{r^2}{\rho_b^2}, \tag{6}$$

where Γ is the upper incomplete gamma function. The approximation in Eq. (6) is reasonably good over the region in the plasma where the beam is extracted, $|r/\rho_b| \leq 1$. Because the leading term in Eq. (6) is quadratic in r, it can be inserted into Eq. (2) and integrated over space in the same manner that led to Eq. (3). Unfortunately, this expression contains ξ, which is an unknown parameter. However, by integrating over $E_\parallel$, an integral expression can be obtained for ξ,

$$\xi = \frac{e^2}{TL_p}\int_{V_E}^{\infty} f(E_\parallel)dE_\parallel. \tag{7}$$

This expression is most conveniently written in terms of ξ, R_W/λ_D, and the parameter

$$\eta \equiv -\frac{e}{T}[V_E - \phi_0(0)]. \tag{8}$$

The result is a universal form valid for all beams, namely,

$$\xi = (1+\xi)\left[\frac{Ae^{-A^2}}{\sqrt{\pi}} - (A^2 - 0.5)\mathrm{erfc}(A)\right], \tag{9}$$

where

$$A = \sqrt{\eta + \xi\left[\gamma + 2\ln\frac{R_W}{\lambda_D} + \Gamma\left(0, \frac{R_W^2}{\rho_b^2}\right)\right]}$$

and γ is the Euler gamma constant. The quantities ξ and η are the suitably scaled values of N_b and V_E, respectively. Thus, for a given initial plasma and value of R_W/λ_D, Eq. (9) relates N_b to V_E. In this case, Eq. (9) can be used to calculate N_b as a function of V_E for fixed values of R_W/λ_D. Although Eq. (9) is a transcendental equation and cannot be solved analytically for $\xi(\eta)$, one can easily find a self-consistent solution numerically at fixed values of R_W/λ_D.

Using Eq. (9), the parallel energy distribution can then be calculated, namely,

$$f(E_\parallel) = -\frac{1}{e}\frac{dN_b}{dV_E}, \tag{10}$$

evaluated at $-eV_E = E_\parallel$. In scaled variables, Eq. (10) becomes

$$f(E_\parallel) = \frac{e^2}{L_p}\frac{d\xi}{d\eta}, \tag{11}$$

evaluated at $\eta = [E_\parallel + e\phi_0(0)]/T$. While taking the derivative of Eq. (9) with respect to ξ can be done analytically, the expression is rather complicated, and so the distributions $f(E_\parallel)$ reported here are calculated numerically.

It should be mentioned again that predictions of both ξ and $f(E_\parallel)$ depend on the assumption stated earlier that particles with largest $E_\parallel$ escape first. Without this assumption, Eq. (7) is invalid and we can no longer predict the energy distribution of the extracted beam.

As will be shown below, the shape of $f(E_\parallel)$ varies significantly as ξ is changed. In order to provide measures of the distribution resulting from these changes, it is useful to calculate the mean and rms energies of the distribution. For most beam applications it is the total energy $E = E_\parallel + E_\perp$ that is of primary importance. We define the mean energy relative to the minimum energy of the beam $E_{\min} = -eV_E$ as

$$\delta\bar{E} = \langle E\rangle - E_{\min} \tag{12}$$

and the dispersion in energy (i.e., rms deviation from the total mean energy) as

$$\Delta E = \sqrt{\langle E^2\rangle - \langle E\rangle^2}. \tag{13}$$

In Eqs. (13) and (14), $\langle\ \rangle$ denotes the average of the quantity over the distribution function $f(E_\parallel, E_\perp)$. These quantities will be calculated below as a function of beam amplitude. In the small beam limit ($\xi \to 0$), $\delta\bar{E} \to 2T$, and $\Delta E \to \sqrt{2}T$; while in the dilute charged gas limit (i.e., the nonplasma limit; $|e\phi_0(0)| \ll T$ and $N_b = N_0$), ΔE and $\delta\bar{E}$ are

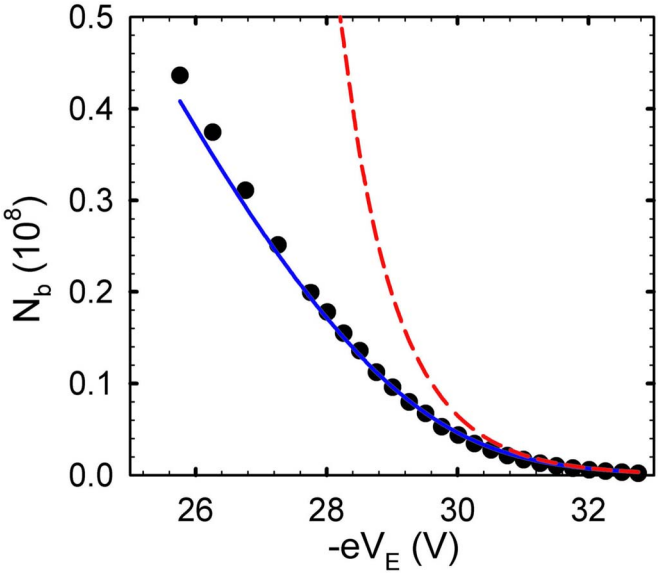

FIG. 5. (Color online) The number of beam particle N_b (solid circles) is shown as a function of the extraction voltage V_E. Here, $T=1.0$ eV, $n_0 \approx 1 \times 10^9$ cm^{-3}, and $\phi_0(0)=27$ V. Also shown are the predictions of Eq. (9) (—) solved numerically along with the solution (- - -) obtained by neglecting ξ on the rhs of the equation.

$\sqrt{3/2}T$ and $(3/2)T$, respectively. The difference between these two cases is that for the former, only the tail of the Maxwellian is extracted as opposed to the entire particle distribution.

IV. COMPARISON BETWEEN THEORY AND EXPERIMENT

Shown in Fig. 5 are data for the beam amplitude (i.e., number of beam particles) N_b extracted as a function of V_E together with two predictions of the theory. The initial plasma parameters were $N=4\times10^8$, $n=1\times10^9$ cm^{-3}, $T=1$ eV, and $L_p=15$ cm. The dashed line is the prediction of Eq. (9) when ξ is neglected on the right-hand side (rhs). This results in a direct expression for ξ when $\Delta\phi(r)$ can be neglected during the beam extraction process (i.e., for small beams). As seen in the figure, these predictions agree with the data for small values of N_b (or ξ); however they diverge rather dramatically for larger values of N_b. Because $\Delta\phi(r)$ acts to inhibit particles from escaping, neglecting it results in a large overestimation of the number of escaping particles. The solid line in Fig. 5 is the prediction of Eq. (9) solved self-consistently with $\phi_0(0)$ adjusted for best fit. In this case, the predictions and the data are in excellent agreement.

The beam parallel energy distribution $f(E_\parallel)$ can be calculated numerically by taking the derivative $dN_b/d(eV_E)$ of the data and predictions shown in Fig. 5 to obtain the experimental and predicted values for $f(E_\parallel)$. For the curve with ξ neglected on the rhs of Eq. (9), this derivative is identical to Eq. (3). The experimental and predicted distribution functions are shown in Fig. 6 for three values of ξ. As shown in Fig. 6(a), for the smallest-amplitude beam ($\xi=0.02$), $\Delta\phi(r)$ can be neglected and the predictions of Eq. (3) agree well with the data. As shown in Figs. 6(b) and 6(c), as ξ increases, the predictions of Eq. (3) deviate significantly from the data. Even for the moderately small value of $\xi=0.1$ [Fig. 6(b)], Eq. (3) does a poor job at predicting $f(E_\parallel)$ due to the nonnegligible effect of $\Delta\phi(r)$. However, as shown in Figs. 6(b) and 6(c), a good agreement is obtained with the predictions using the derivative to the full solution in Eq. (9), even for relatively large beams (e.g., $\xi=0.4$). The corresponding values of $\Delta E/T$ ($\delta\bar{E}/T$) for the distributions shown in Fig. 6 are 1.4 (2.0), 1.5 (2.25), and 1.8 (3) for $\xi=0.02$, 0.1, and 0.4, respectively.

With this validation of the predictions of Eq. (9), we consider further its implications for a wide range of plasma parameters and beam amplitudes. Equation (9) relates ξ to η with the only adjustable constant being the dimensionless parameter R_W/λ_D. Given R_W/λ_D, one can then solve for ξ as a function of η, relating the beam amplitude N_b to the extraction voltage V_E for given values of the plasma parameters (i.e., T, n, and L_p). In Fig. 7(a), the solutions in Eq. (9) are shown for three values of R_W/λ_D spanning a factor of 100 in this parameter. The data from Fig. 5 are scaled appropriately and included for reference. As can be seen in Fig. 7(a) and by examining Eq. (9), the curves have a noticeable but relatively weak dependence on R_W/λ_D.

The distribution function can then be obtained from the solutions for $\xi(\eta)$ using Eq. (11). Results are shown in Fig. 7(b) for $\xi=0.4$ and the three values of R_W/λ_D shown in Fig. 7(a). These energy distributions vary markedly in shape as R_W/λ_D is increased. Useful measures of the changes in the distribution function are obtained by calculating the moments [Eqs. (12) and (13)] of the distribution given by Eqs. (9) and (11). In Fig. 8(a), the mean beam energy $\delta\bar{E}/T$ is shown as a function of ξ for a range of R_W/λ_D. This is a critical parameter for many applications. Also shown in Fig. 8(a) are the measured data for $R_W/\lambda_D=50$, which are in good agreement with the predictions.

In Fig. 8(b) the calculated rms energy spread $\Delta E/T$ is shown as a function of ξ for the same values of R_W/λ_D as in Fig. 8(a). Experimental data for $R_W/\lambda_D=50$ are also shown and are in good agreement with the predictions. For applications where good energy resolution is required, it is desirable to have as small a value of ΔE as possible. While increasing the beam amplitude increases ΔE, for plasmas with smaller R_W/λ_D, this has a diminishing effect. The reason for this can be seen by approximating $\Delta\phi(0)$ as that from a flat top and then expressing it as

$$\left|\frac{e\Delta\phi(0)}{T}\right| \approx \xi\left[1+2\ln\frac{R_W}{\lambda_D}-\ln 4(1+\xi)\right]. \tag{14}$$

The increase in the rms spread in ΔE is related to the number of particles that is prevented from escaping at $r=0$ by the change in plasma potential $\Delta\phi$ and is only a function of ξ and R_W/λ_D. Notice that for a given ξ as R_W/λ_D increases, so does $e\Delta\phi/T$. Physically, this can happen either by decreasing λ_D and thus making the beam smaller, thereby increasing the beam potential, or by increasing R_W which decreases the effect of the screening image charge from the cylindrical electrode on the beam potential. Increasing $\Delta\phi$ will prevent more particles from escaping, thus increasing the energy spread of the resulting beam (cf. Fig. 7).

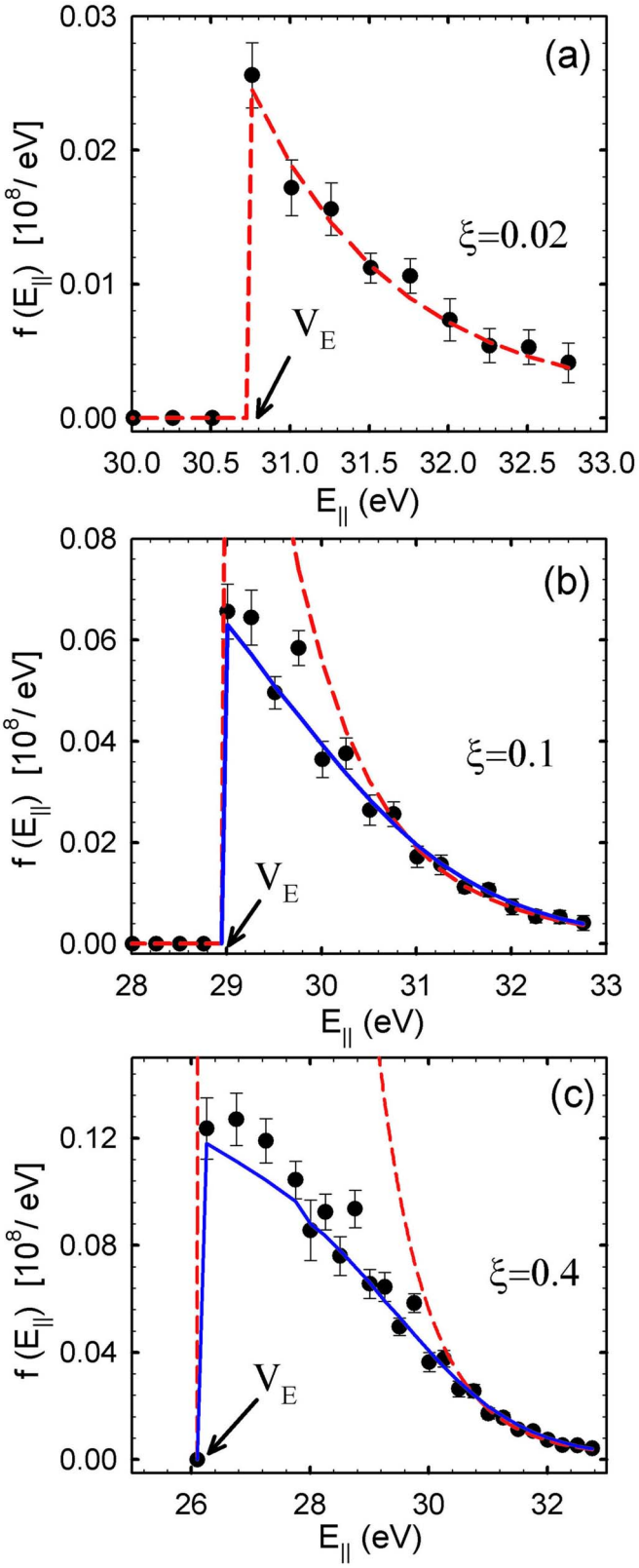

FIG. 6. (Color online) Comparison of the energy distributions for different beam amplitudes ξ: (a) 0.02, (b) 0.1, and (c) 0.4. These distributions were obtained from Eq. (10) using the experimental data and the theoretical predictions shown in Fig. 5. The experimental conditions and symbols are the same as in Fig. 5.

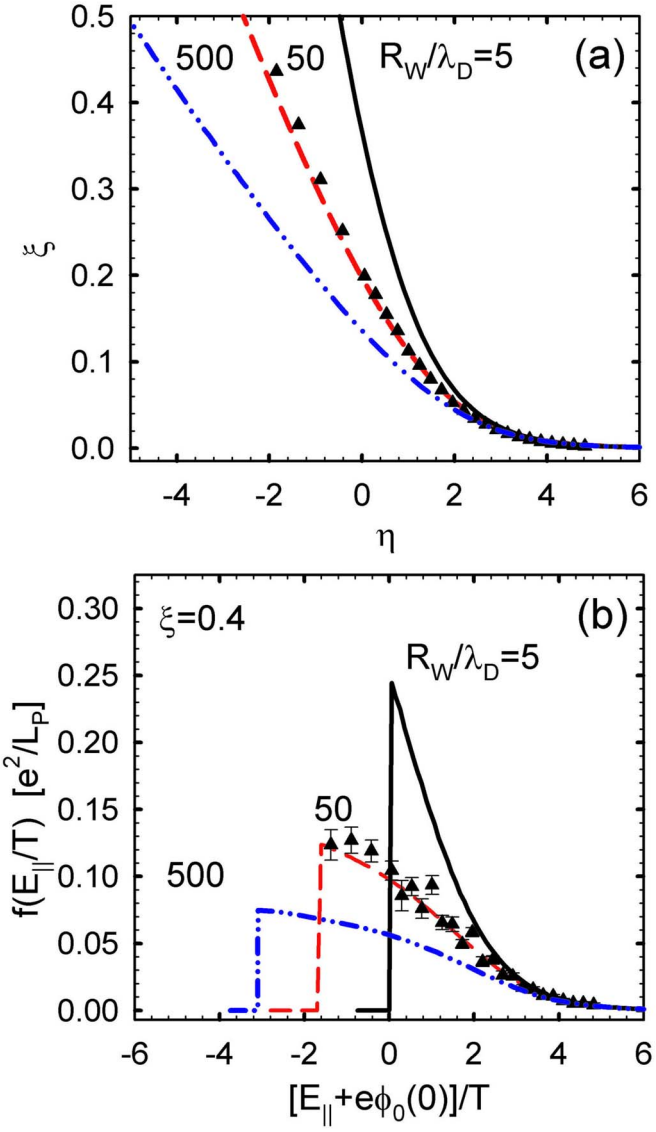

FIG. 7. (Color online) (a) Numerical solutions in Eq. (9) (—, - - -, ···) are shown for values of R_W/λ_D of 5, 50, and 500, respectively. (b) The corresponding distribution functions $f(E_\parallel)$ are shown scaled by $(e^2/L_p)^{-1}$ calculated with Eq. (11) using the solutions shown in (a). Data from Figs. 5 and 6(c) (▲) are also plotted in (a) and (b).

Note that in Fig. 8, as ξ increases the spread in $E_\perp$ remains constant, so it is only the parallel energy distribution that contributes to the increase in the mean energy and the dispersion $\Delta E/T$. In particular, the dispersion in the parallel energies is

$$\frac{\Delta E_\parallel}{T} = \sqrt{\left(\frac{\Delta E}{T}\right)^2 - 1}, \tag{15}$$

providing a convenient relation between ΔE and $\Delta E_\parallel$. This parameter increases from 0.9 to 1.5 as ξ increases from 0.02 to 0.4 in the data shown in Fig. 6.

For completeness, the predicted and measured values of the beam width ρ_b as a function of ξ are shown in Fig. 8(c).[11] This parameter is critical for beam applications where spatial resolution is required. Figure 8(c) shows a good agreement

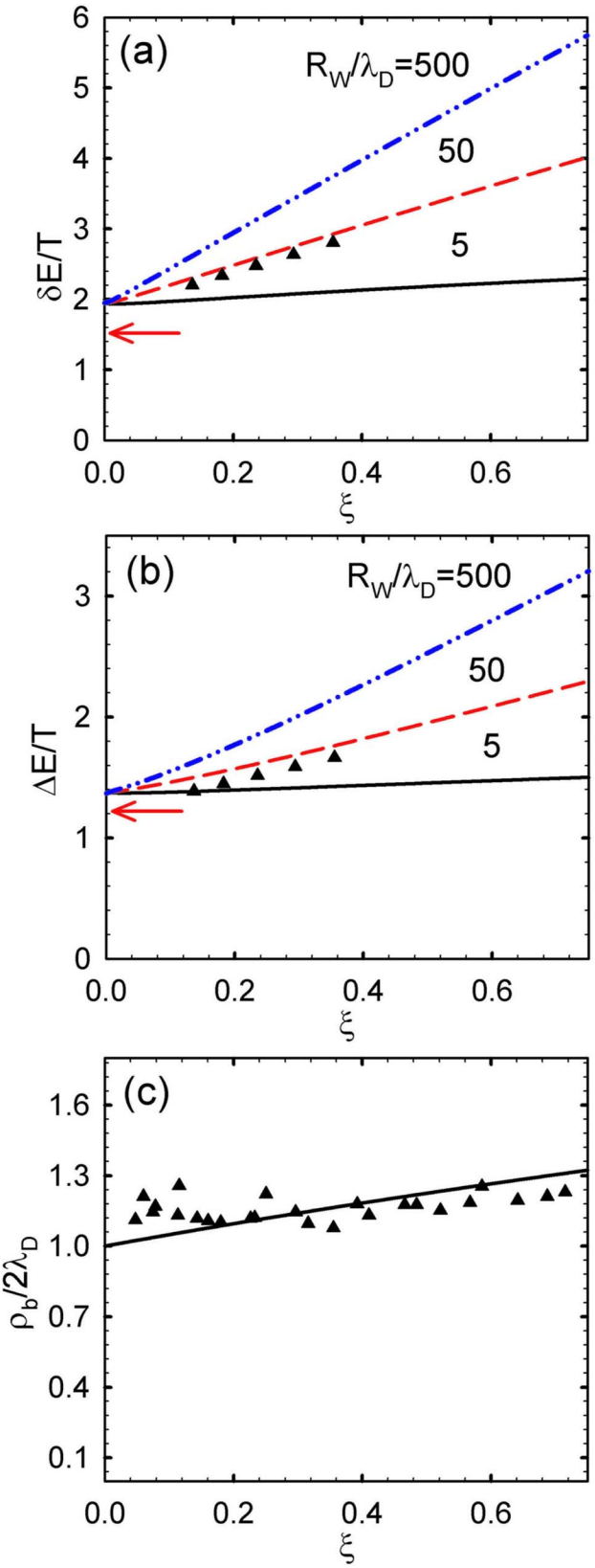

FIG. 8. (Color online) The quantities of (a) the mean energy $\delta\bar{E}/T=\langle E-E_{\min}\rangle/T$ (i.e., $E_{\min}=-eV_E$); (b) rms spread in total energy $\Delta E/T$ calculated using Eqs. (9) and (11)–(13) is shown as a function of ξ for three values of R_W/λ_D; and (c) the scaled value of the beam radius $\rho_b/(2\lambda_D)$ (—) is shown as a function of ξ [from Eq. (5)]. Data for plasma parameters given in Fig. 5 (▲) are also shown for $R_W/\lambda_D=50$. Arrows indicate the value for the extraction of an entire Maxwellian distribution in the dilute charged gas limit, $|e\phi_0(0)|\ll T$ and $N_b=N_0$. Curves are marked the same as in Fig. 7. See text for details.

between measured and predicted beam widths and that this width remains near the minimum value of $4\lambda_D$ for the range of ξ values investigated here.

Finally, it is not uncommon in applications to encounter situations where the magnetic field is changed adiabatically from some value B_i to another value B_f between the trap and some other location where the beam is used. In this case, the quantity $E_\perp/B$ is an adiabatic invariant, and so values of $E_\perp$ transform as $E_{\perp f}=E_{\perp i}(B_f/B_i)$. Since the total particle energy remains constant, $E_{\|f}=E_{\|i}+E_{\perp i}(1-B_f/B_i)$. Additionally, since the magnetic flux is conserved, the beam radius ρ_b will vary as $B^{-1/2}$.

V. CONCLUDING REMARKS

Previously, a technique was demonstrated to extract beams from non-neutral plasmas in Penning–Malmberg traps, and a simple model was developed to predict the transverse spatial profiles of the extracted beams.[10,11] Here, using an extension of this model, an equation is developed that predicts successfully the beam amplitudes and energy distributions as a function of the extraction voltage for given values of the plasma parameters. This expression conveniently relates ξ to η with the only remaining parameter being the scaled electrode radius R_W/λ_D.

These results, when combined with the previous work, provide quantitative predictions for key beam parameters, namely, the transverse spatial width, the mean beam energy, and rms energy spread. These predictions were successfully verified by experimental measurements. The key results are that the mean beam energy and the rms energy spread increase monotonically by modest amounts as a function of the beam amplitude, while the spatial width is approximately constant near the minimum diameter $2\rho_b=4\lambda_D$. The major variation occurs in the shape of the energy distribution function, which varies markedly with increasing beam amplitude.

This beam-formation technique and the results presented here can be expected to be useful in a variety of applications. In particular, in cases where brightness enhancement is desired, such as positron microscopic studies of materials, the work presented here suggests the following scenario. Positrons from a variety of sources, including electron accelerators, reactors, or radioactive sources, can be accumulated efficiently in a buffer gas trap and then transferred to a high-magnetic-field UHV trap for further manipulation and delivery. Thus trapped plasmas formed can be compressed radially and cooled then further brightness enhanced by extraction from near the magnetic center line as described here. Additional brightness enhancement could then be accomplished by extraction from the magnetic field, electrostatic focusing, and remoderation as necessary.[29]

In other applications, it is the spread in total energy of the beam ΔE which is of primary importance. One example is positron-impact excitation of molecules, clusters and solids. The methods described here have the potential to enable high-resolution studies of vibrational and rotational energy levels. This could be done with either a magnetically guided beam or an electrostatic beam, each of which has certain advantages depending upon the particular measurement.[15]

A powerful technique to study materials is positron annihilation lifetime spectroscopy. In this case, it is desirable to create bursts of positrons with time durations shorter than $\Delta t \sim 100$ ps so that the pulses themselves can be used as the start signal for timing. In this case, a limiting factor to pulse compression is the parallel energy spread of the beam (i.e., $\Delta t \propto \sqrt{\Delta E_{\|}}$).[1,21] Using the techniques described here, $\Delta E_{\|}$ can be reduced to approximately the plasma temperature. Use of a cryogenic plasma then offers the possibility of creating high-quality short bursts of positrons for PALS and similar applications.

It is also possible that the techniques described here could be useful in the formation of cold antihydrogen in the scheme of combining antiproton and positron plasmas in a nested-Penning-trap geometry. One potential impediment to achieving this goal is the velocity imparted to the antiprotons due to the $E \times B$ rotation they experience from the space charge electric field of the dense positron plasma. Since this $E \times B$ rotation velocity increases proportionally to the distance from the axis of symmetry, the center-line extraction method could be applied to one of the species to help mitigate this effect.

In Ref. 11, a method was described to produce an electrostatic beam (i.e., a beam in a region where $B=0$). Further narrowing of the transverse extent of the beam can then be done, for example, using electrostatic focusing techniques. The energy spread of such a beam will be determined by the considerations discussed here. In particular, in the example in Table I of Ref. 11, a value of $\xi=0.1$ was chosen to maintain a beam of narrow spatial extent. As indicated in Figs. 6(b) and 8(a), in this case the parallel energy spread corresponds to $\Delta E_{\|}/T \leq 1$ (i.e., the total energy spread is $1 \leq \Delta E/T \leq 2$), which is consistent with the value assumed in Ref. 11.

For completeness, we note that our previous work to create cold positron beams[6,7] used a distinctly different beam-extraction technique. Positrons were trapped and cooled in a Penning–Malmberg buffer-gas trap to a temperature of 300 K (25 meV), then the bottom of the confining potential well was raised in a pulsed manner to extract beam pulses. In that case, no attempt was made to create a beam of small transverse spatial extent. Empirically, it was found that this nonequilibrium extraction protocol produces a Gaussian energy distribution (i.e., a distinctly different distribution than those discussed here) with a parallel energy spread of 18 meV, full width at half maximum, while the distribution in energies perpendicular to the field remains Maxwellian with an energy spread equal to the temperature of the parent plasma (25 meV). The underlying physical origin of this Gaussian distribution in parallel energies is not currently understood but is possibly due to the nonequilibrium nature of the extraction method used. Both that technique and the one described here can be used to obtain cold beams with energy spreads of the order of the plasma temperature. The advantage of the technique described here is that one can create beams with *both* small transverse size and a narrow energy distribution.

ACKNOWLEDGMENTS

We wish to acknowledge the helpful conversations with R. G. Greaves and P. Bowe and the expert technical assistance of E. A. Jerzewski. This work was supported by the NSF, Grant Nos. PHY 03-54653 and PHY 07-13958.

[1] A. P. Mills, Jr., Appl. Phys. (Berlin) **22**, 273 (1980).
[2] P. Hommelhoff, Y. Sortais, A. Aghajani-Talesh, and M. A. Kasevich, Phys. Rev. Lett. **96**, 077401 (2006).
[3] Y. Yamazaki, Mater. Sci. Forum **445-446**, 430 (2004).
[4] W. E. King, G. H. Campbell, A. Frank, B. Reed, J. F. Schmerge, and B. J. Siwick, J. Appl. Phys. **97**, 111101 (2005).
[5] A. David, G. Kogel, P. Sperr, and W. Triftshäuser, Phys. Rev. Lett. **87**, 067402 (2001).
[6] S. J. Gilbert, C. Kurz, R. G. Greaves, and C. M. Surko, Appl. Phys. Lett. **70**, 1944 (1997).
[7] C. Kurz, S. J. Gilbert, R. G. Greaves, and C. M. Surko, Nucl. Instrum. Methods Phys. Res. B **143**, 188 (1998).
[8] D. B. Cassidy, S. H. M. Deng, R. G. Greaves, and A. P. Mills, Jr., Rev. Sci. Instrum. **77**, 073106 (2006).
[9] C. M. Surko and R. G. Greaves, Phys. Plasmas **11**, 2333 (2004).
[10] J. R. Danielson, T. R. Weber, and C. M. Surko, Appl. Phys. Lett. **90**, 081503 (2007).
[11] T. R. Weber, J. R. Danielson, and C. M. Surko, Phys. Plasmas **13**, 123502 (2008).
[12] N. Oshima, R. Suzuki, T. Ohdaira, A. Kinomura, T. Narumi, A. Uedono, and M. Fujinami, J. Appl. Phys. **103**, 094916 (2008).
[13] J. Sullivan, S. J. Gilbert, and C. M. Surko, Phys. Rev. Lett. **86**, 1494 (2001).
[14] J. P. Marler and C. M. Surko, Phys. Rev. A **72**, 062702 (2005).
[15] C. M. Surko, G. F. Gribakin, and S. J. Buckman, J. Phys. B **38**, R57 (2005).
[16] A. P. Mills, Jr., Science **218**, 335 (1982).
[17] P. J. Schultz and K. G. Lynn, Rev. Mod. Phys. **60**, 701 (1988).
[18] D. Schodlbauer, P. Sperr, G. Kogel, and W. Trifthauser, Nucl. Instrum. Methods Phys. Res. B **34**, 258 (1988).
[19] K. Fallstrom and T. Laine, Appl. Surf. Sci. **149**, 44 (1999).
[20] R. Suzuki, Radiat. Phys. Chem. **58**, 603 (2000).
[21] R. G. Greaves, S. J. Gilbert, and C. M. Surko, Appl. Surf. Sci. **194**, 56 (2002).
[22] N. Alberola, T. Anthonioz, A. Badertscher, C. Bas, A. S. Belov, P. Crivelli, S. N. Gninenko, N. A. Golubev, M. M. Kirsanov, A. Rubbia, and D. Sillou, Nucl. Instrum. Methods Phys. Res. A **560**, 224 (2006).
[23] D. B. Cassidy, S. H. M. Deng, H. K. M. Tanaka, and A. P. Mills, Appl. Phys. Lett. **88**, 194105 (2006).
[24] G. Gabrielse, N. S. Bowden, P. Oxley, A. Speck, C. H. Storry, J. N. Tan, M. Wessels, D. Grzonka, W. Oelert, G. Schepers, T. Sefzick, J. Walz, H. Pittner, T. W. Hansch, and E. A. Hessels, Phys. Rev. Lett. **89**, 233401 (2002).
[25] M. Amoretti, C. Amsler, G. Bonomi, A. Bouchta, P. Bowe, C. Carraro, C. Cesar, M. Charlton, M. J. T. Collier, M. Doser, V. Filippini, K. S. Fine, A. Fontana, M. C. Fujiwara, R. Funakoshi, P. Genova, J. S. Hangst, R. S. Hayano, M. H. Holzscheiter, L. V. Jørgensen, V. Lagomarsino, R. Landua, D. Lindelöf, E. Lodi-Rizzini, M. Macrì, N. Madsen, G. Manuzio, M. Marchesotti, P. Montagna, H. Pruys, C. Regenfus, P. Riedler, J. Rochet, A. Rotondi, G. Rouleau, G. Testera, A. Variola, T. L. Watson, and D. P. van der Werf, Nature (London) **419**, 456 (2002).
[26] D. L. Eggleston, C. F. Driscoll, B. R. Beck, A. W. Hyatt, and J. H. Malmberg, Phys. Fluids B **4**, 3432 (1992).
[27] G. W. Hart and B. G. Peterson, Phys. Plasmas **13**, 022101 (2006).
[28] J. Aoki, Y. Kiwamoto, and Y. Kawai, Phys. Plasmas **13**, 112109 (2006).
[29] A. P. Mills, Jr., Appl. Phys. (Berlin) **23**, 189 (1980).